

Article

Comparison of the Physicochemical Properties of TiO₂ Thin Films Obtained by Magnetron Sputtering with Continuous and Pulsed Gas Flow

Artur Wiatrowski ¹, Michał Mazur ^{1,*}, Agata Obstarczyk ¹, Damian Wojcieszak ¹,
Danuta Kaczmarek ¹, Jerzy Morgiel ² and Des Gibson ³

¹ Faculty of Microsystem Electronics and Photonics, Wrocław University of Science & Technology, Janiszewskiego 11/17, 50-372 Wrocław, Poland; artur.wiatrowski@pwr.edu.pl (A.W.); agata.obstarczyk@pwr.edu.pl (A.O.); damian.wojcieszak@pwr.edu.pl (D.W.); danuta.kaczmarek@pwr.edu.pl (D.K.)

² Institute of Metallurgy and Materials Science, Polish Academy of Sciences, Reymonta 25, 30-059 Cracov, Poland; j.morgiel@imim.pl

³ Scottish Universities Physics Alliance (SUPA), Institute of Thin Films, Sensors & Imaging, University of the West of Scotland, High Street, Paisley PA1 2BE, UK; des.gibson@uws.ac.uk

* Correspondence: michal.mazur@pwr.edu.pl; Tel.: +48-71-320-3322

Received: 31 August 2018; Accepted: 19 November 2018; Published: 20 November 2018



Abstract: In this paper, a comparison of TiO₂ thin films prepared by magnetron sputtering with a continuous and pulsed gas flow was presented. Structural, surface, optical, and mechanical properties of deposited titanium dioxide coatings were analyzed with the use of a wide range of measurement techniques. It was found that thin films deposited with a gas impulse had a nanocrystalline rutile structure instead of fibrous-like anatase obtained with a continuous gas flow. TiO₂ thin films deposited with both techniques were transparent in the visible wavelength range, however, a much higher refractive index and packing density were observed for coatings deposited by the pulsed gas technique. The application of a gas impulse improved the hardness and scratch resistance of the prepared TiO₂ thin films.

Keywords: gas impulse magnetron sputtering; thin films; TiO₂; microstructure; surface properties; optical properties; mechanical properties; hardness; scratch resistance

1. Introduction

Thin oxide films can be prepared by various methods, such as chemical vapor deposition, electron beam evaporation, direct current or radio frequency magnetron sputtering, arc deposition, atomic layer deposition, and sol-gel [1–4]. Thin films prepared in physical vapor deposition (PVD) processes exhibit numerous advantages over coatings deposited by other aforementioned methods, that is, they have controlled homogeneity and thickness over a large area [5,6]. In the case of the magnetron sputtering technique, especially pulsed methods have recently gained a great interest because they allow the creation of conditions for the growth of thin films that are difficult (or impossible) to achieve in standard (continuous, direct current) sputtering processes. The most important factor is the generation of plasma that is more energetic and usually of higher density with respect to the plasma of continuous, direct current processes [7]. The presence of high-density energetic plasma during the deposition process results in a high degree of sputtered material ionization and the possibility of directing a high-density ion flux to the growing film. The technological outcome of that is the possibility of obtaining layers with a very smooth surface and a very dense structure, that is, with much smaller grains as compared to layers deposited during continuous, direct current sputtering processes. The high-density energetic

plasma of pulsed magnetron sputtering processes is generated during the pulses in the discharge presence. The process of the pulsed magnetron sputtering can be achieved in two ways: (i) using an impulse (medium frequency MF or pulsed-DC) waveform of the electrical signal supplying the cathode of the magnetron, or (ii) using an impulse dosing of the gas to the deposition chamber.

In the case of the pulsed magnetron sputtering realized by impulse electrical signal supplying the cathode with momentary discharge voltage (and thus the discharge current and discharge power), the obtained values may significantly exceed the ones typically reached in standard sputtering processes. Momentary discharge power can be set in the range from 1 kW to even 1 MW. The duration of a single sputtering pulse is short (μs – ms) and pulse repetition is rather low, in the range from Hz to a few kHz. Because of this, the average discharge power is at the level typical of standard sputtering processes and therefore a standard magnetron can still be used. Unfortunately, the sequential ignition and decay of the sputtering discharge reduce the deposition rate of the films [7,8]. This reduction is the result of three main factors [7,9]: (i) high target power density during the individual sputtering pulse that creates conditions for the occurrence of the self-sputtering phenomenon, (ii) the sputtering yield does not scale linearly with the cathode voltage, and (iii) the sputtering of the cathode stops between pulses. During the continuous, direct current sputtering processes, the limitation of the high-density energetic plasma generation capability is the current-voltage characteristic of the glow discharge generated by the magnetron source. It is not possible to increase the anode–cathode voltage (that influences the plasma particles energy) without a significant increase in the discharge current and therefore in the discharge power [10]. The high target power density causes problems with the target cooling and stability of sputtering as the arcing is likely to take place during standard, direct current processes [11].

Moreover, in the case of the pulsed magnetron sputtering realized by the usage of gas impulse dosing to the deposition chamber, the whole gas mixture (working and reactive gas) or only the selected component (reactive gas) may be pulsed. The sequential injection of gas portions causes a cyclic change of pressure conditions in the chamber. Before the next pulse of the gas, the pressure is lower than normal, which reduces the number of collisions and energy loss of the particles directed to the substrate [12–15]. Recently, there has also been some interest in a new modification of the sputtering method called gas impulse magnetron sputtering (GI MS) [16–19]. In the case of this method, fast changes in working gas pressure lead to the thermal unequilibrium of plasma. Additionally, the pressure during the GI MS process is reduced and therefore the dissipation of the kinetic energy of sputtered particles is significantly decreased due to the collision with gas. Furthermore, such a modification causes the elongation of the mean free path of sputtered particles as compared to processes conducted with the continuous flow of working and reactive gases. Therefore, thin films deposited with the use of the GI MS method may exhibit improved properties (e.g., durability, mechanical or optical properties).

In this paper, the structural, surface, optical, and mechanical properties of TiO_2 thin films deposited by two different magnetron sputtering methods (with a continuous gas flow and with a gas impulse) have been compared. Titanium dioxide was selected as a well-known material in electronics and optoelectronics [20–23]. It is frequently used for the preparation of, for example, optical coatings. The properties of TiO_2 can be modified with the change of structure, which usually can be obtained by the modification of deposition process parameters, doping, or by additional annealing in high temperature. It is worth emphasizing that the application of the pulsed gas technique offers a possibility to prepare high-quality optical coatings with high hardness.

2. Materials and Methods

TiO_2 thin films were deposited by two various magnetron sputtering techniques: medium frequency (denoted as MF MS) and gas impulse (denoted as GI MS). The main difference between the two used sputtering techniques was the change of the pressure during the deposition process, which was a result of applied gas-supplying mode. In the MF MS process, which was conducted with a continuous gas flow of 18 sccm ensured by an MKS mass-flow controller, the pressure was kept at the

level of 2×10^{-2} mbar. This was the lowest value that allowed the plasma discharge to be sustained. Moreover, in the GI MS process, the average deposition pressure was ten times lower and, similarly as in the case of the MF MS process, it was the lowest value that allowed the pulsed plasma discharge to be received. In the GI MS technique, gas was injected directly on the target by a Festo fast valve in short (few ms) pulses with a frequency of 1 Hz, which caused the initiation of a glow discharge (injection of small gas portions which did not lead to a continuous discharge). Additionally, the powering of the magnetron was synchronized with gas pulses and in each cycle lasted 100 ms. The other sputtering conditions remained the same for the MF MS and GI MS processes. In both techniques, during the deposition, high-purity metallic titanium targets were sputtered with the use of a DPS (Dora Power Systems) power supply working in a unipolar mode at the frequency of 165 kHz of sinusoidal pulses with the voltage amplitude of 1.8 kV. In the case of both processes, metallic Ti targets were sputtered in pure oxygen, without argon acting as a working gas. The sputtering apparatus was equipped with diffusion and rotary pumps. Before both processes, the vacuum chamber was evacuated to a base pressure of ca. 5×10^{-5} mbar. Both deposition processes were conducted for 240 min. Thickness was measured using the Taylor Hobson optical profiler, and for the TiO₂ thin films deposited by MF MS, it was equal to 580 nm, while the coatings from the GI MS process were 300 nm thick. The difference in the final thickness resulted directly from the gas supply mode, however, the obtained values were sufficient to conduct further studies of various properties of both thin films.

Thin films were deposited on various substrates, including silicon, fused silica, and Ti6Al4V metallic alloys due to different measurement methods used to determine the properties of TiO₂. XRD and optical properties measurements were performed using thin films deposited on fused silica, while surface morphology and cross section were analysed with the use of coatings sputtered on silicon. Moreover, thin films deposited on silica and Ti6Al4V titanium alloys were employed in mechanical analysis. Fused silica and silicon substrates were polished and, as a result, their surface roughness (R_q) was below 1 nm. The surface of titanium alloys was polished on emery papers and diamond suspension up to 0.05 μm to a “mirror image” and their R_q was also below 1 nm (as measured by an optical profiler).

Structural properties were analyzed using X-ray diffraction (XRD), Raman spectroscopy, and transmission electron microscopy (TEM). XRD measurements were performed employing PANalytical Empyrean PIXel3D powder diffractometer (Malvern Panalytical Ltd., Royston, UK) with Cu K α X-ray ($\lambda = 1.54056 \text{ \AA}$). The average crystallite sizes were calculated with respect to Debye–Scherrer’s equation from the full width at half maximum (FWHM) of a peak, taking into consideration the broadening of the XRD apparatus. The crystallites’ size was also evaluated using MDI Jade 5.0 software. Raman spectroscopy measurements were carried out with the aid of a Thermo Fisher Scientific DXRTM Raman Microscope (Thermo Fisher Scientific, Waltham, MA, USA) using a 455 nm blue laser diode at a power of 6 mW and the exposure time of 10 s. The TECNAI G² FEG Super-Twin (200 kV) transmission electron microscope (Thermo Fisher Scientific, Waltham, MA, USA) was used for the detailed analysis of the crystal structure of TiO₂ coatings.

Surface properties were determined by scanning electron microscopy (SEM), atomic force microscopy (AFM), X-ray photoelectron spectroscopy (XPS), and wettability measurements. Surface and cross-sectional morphology were estimated with the use of FEI Helios NanoLab 600i SEM (Thermo Fisher Scientific, Waltham, MA, USA). A UHV VT AFM/STM Omicron AFM (Scienta Omicron, Taunusstein, Germany), which operated in ultrahigh vacuum conditions in a contact mode, was used to evaluate surface roughness. The surface chemical states of TiO₂ thin films were determined using a Specs Phoibos 100 MCD-5 hemispherical analyzer (Specs, Berlin, Germany) using a Specs XR-50 X-ray source with Mg K α (1253.6 eV) beam. A standard operation of calibrating all obtained XPS spectra to the binding energy of adventitious C1s peak at 284.8 eV was conducted. Wettability measurements were performed with the aid of an Attension Theta Lite tensiometer (Biolin Scientific, Gothenburg, Sweden) using deionized water, ethylene glycol, and ethanol for the evaluation of a contact angle.

Transmittance and reflectance spectra were measured at a 30° angle of incident light for both S and P polarisation using an Aquila nkd-8000 spectrophotometer (Aquila Instruments Limited, Essex, UK). On the basis of the obtained results, the refractive index and extinction coefficient were determined with the aid of FilmStar software employing an extended Cauchy model for coatings with extinction coefficient >0 . Transmission spectra were also measured with the use of an Ocean Optics QE65000 spectrophotometer (Ocean Optics, Largo, FL, USA) to evaluate the fundamental absorption edge, optical band gap energy (E_g) for indirect transitions, and Urbach energy.

In the case of the mechanical properties of the deposited thin films, the hardness and Young's elastic modulus were analyzed by nanoindentation using the method proposed by Oliver and Pharr [24]. Measurements were performed with the use of a CSM Instruments nanoindenter (Needham, MA, USA) equipped with a diamond Vickers tip. The scratch resistance of the coatings was measured with the use of a Taber Oscillating Abrasion Tester 6160 (Taber Industries, North Tonawanda, NY, USA) according to the ASTM F735 standard [25]. The surface of TiO₂ thin films was examined for scratch resistance by an Olympus BX51 optical microscope (Olympus, Tokyo, Japan) and with the aid of a TalySurf CCI Lite Taylor Hobson optical profiler (Taylor Hobson, Leicester, UK).

3. Results

3.1. Microstructure

XRD studies performed for both samples revealed significant differences in the microstructure of coatings deposited by MF MS and GI MS. The diffraction pattern of the first one showed intense peaks related to the anatase phase of TiO₂, while the latter exhibited only a small peak related to the TiO₂-rutile phase. It was also found that the TiO₂-rutile thin films were textured among (110) crystal plane. Small shifts between the diffraction peaks of deposited coatings and standard values from PDF cards [26,27] could indicate negligible stresses that might occur in the microstructure [28–30]. It was found that thin films with the anatase phase had crystallites of ca. 36 nm size, while for the rutile one, their size was more than three times smaller. However, taking into consideration low signal-to-noise ratio in the case of coatings deposited by the GI MS process, this calculation could be encumbered with a slight error. XRD patterns are shown in Figure 1. The detailed results of the XRD measurements of TiO₂ thin films deposited by MF MS and GI MS are shown in Table 1.

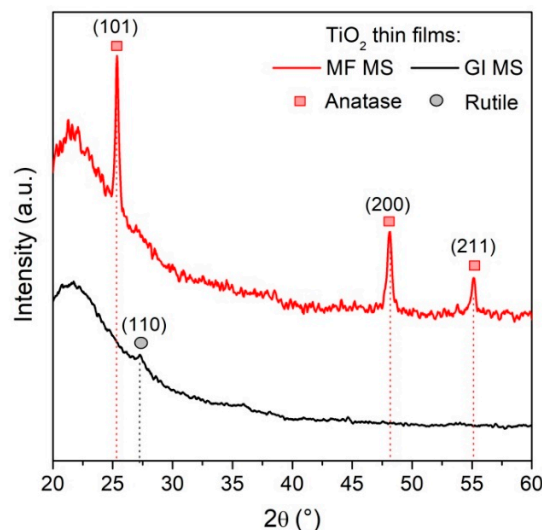


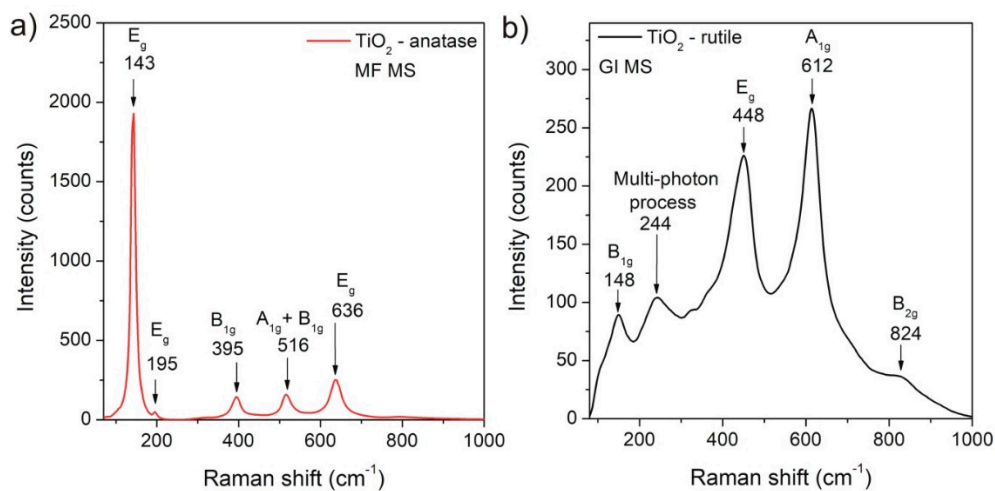
Figure 1. XRD measurement results of TiO₂ thin films deposited by MF MS and GI MS.

Table 1. XRD measurement results of TiO₂ thin films deposited by MF MS and GI MS.

Thin Film	Phase	Crystal Plane	<i>D</i> (nm)	<i>d</i> (nm)
PDF No. 21-1272 TiO ₂	anatase	-	-	0.3520
TiO ₂ (MF MS)	anatase	(101)	36.1	0.3511
PDF No. 21-1276 TiO ₂	rutile	-	-	0.3247
TiO ₂ (GI MS)	rutile	(110)	11.0	0.3266

D—average crystallite size, *d*—interplanar distance.

Raman spectroscopy was used in order to further investigate the microstructure of deposited coatings since it is a method sensitive to the crystalline phases that occur in thin films even if they are also composed of a vast amount of an amorphous phase. Both anatase and rutile phases of titanium dioxide are tetragonal and have six and four active modes occurring at specified Raman shifts, respectively [31–34]. Raman spectra of TiO₂ thin films deposited by MF MS and GI MS are shown in Figure 2a,b, respectively. The obtained results are in good agreement with the reference values for the anatase and rutile phases. In both cases, peaks were sharp and had high intensity which can be considered as the proof of a highly crystalline microstructure occurring in the deposited thin films.

**Figure 2.** Raman spectra of the as-prepared TiO₂ thin films from: (a) MF MS (anatase); (b) GI MS (rutile).

The investigation of the microstructure of the deposited thin films was completed by TEM measurements (Figure 3). Bright field (BF) images of the coating deposited by MF MS with a continuous gas flow revealed that the film had a fibrous structure. Immediately after the deposition, this thin film was very well crystallized with a small number of defects. In the bright field image (Figure 3a), voids or amorphous areas with locally lower density between the fibers were marked with red lines. Those voids were formed due to the inhomogeneity of crystallized grains. The analysis of the selected area electron diffraction confirmed the results obtained with XRD and Raman that the thin film had a nanocrystalline anatase structure. Electron diffraction (shown as an inset in the bright field image with marked crystal planes) had a rather spotted character, which was proof of very good crystallization of the film with large crystallites and indicated strong texture. High-resolution TEM (HRTEM) images confirmed once more that the coating had a fine nanocrystalline anatase phase. The FFT diffraction pattern (added as an inset to the HRTEM image) was obtained from the crystallite, which was free of defects and allowed for an accurate evaluation of the separation of planes and the angle between them that indicated the anatase phase of [11–1] zone axis. Additionally, HRTEM images confirmed the presence of voids between the fibers.

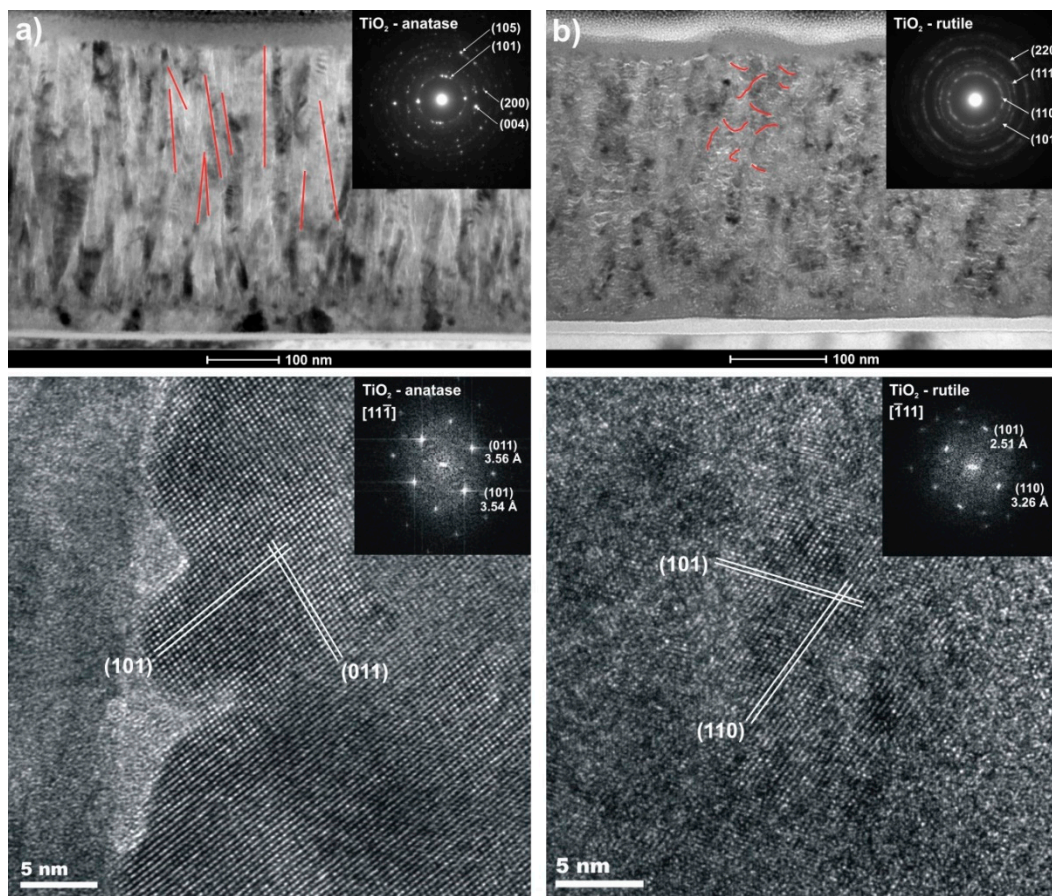


Figure 3. Bright field and HRTEM images of the cross section of as-deposited TiO₂ thin films from: (a) MF MS; (b) GI MS processes.

In the case of thin films deposited by gas impulse magnetron sputtering, the bright field TEM images (Figure 3b) revealed that the grains in the coating had significantly lower dimensions. The microstructure was much more defected and the defects were nonuniform. The amorphous and void areas were marked with red lines in the BF image. The selected area diffraction pattern confirmed that the coating consisted of a nanocrystalline rutile phase. In contrast to the anatase thin film, the electron diffraction was composed of fuzzy rings, meaning that the microstructure was built up from nanosized crystallites with various orientations. The HRTEM investigations (Figure 3b) showed that the crystallites of low-indexed rutile planes were very small and their size was ca. 10 nm, which is consistent with the XRD results. The crystallites were much more defective as compared to the anatase thin films and the refinement of the microstructure was observed. The structure had a pseudocolumnar character and each column was composed of several small grains. The HRTEM image showed the visible lattice fringe spacings of 3.26 Å and 2.51 Å, which comply with the separation of (101) and (110) planes, respectively, within the rutile $[-111]$ zone axis.

3.2. Surface Properties

The surface properties of the deposited TiO₂ thin films were determined with the use of SEM, AFM, XPS, and wettability measurements. The results of the SEM studies of TiO₂ thin films deposited with a continuous gas flow (Figure 4a) showed that its surface was crack-free, composed of large size, visible grains tetragonal in shape. Moreover, all grains had a similar size and the surface was homogeneously covered with them. The cross-sectional image revealed the presence of elongated, fibrous grains and voids between them. Additionally, the thickening of the grains with the growth of the coating was observed. In the case of the rutile thin film deposited with a gas impulse (Figure 4b),

its surface was also crack-free and homogenous, however, some small variations of topography were also observed. The cross-sectional image was significantly different as compared to the anatase thin film. The rutile coating did not have a fibrous-like microstructure and seemed to be composed of grains, which seems to confirm the TEM results.

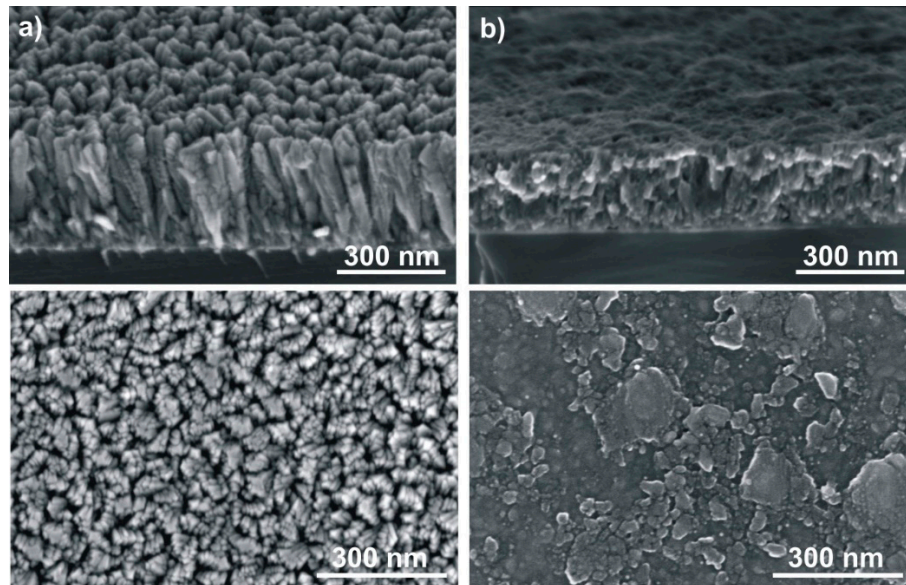


Figure 4. SEM images of the cross section and surface of as-deposited TiO₂ thin films obtained in: (a) MF MS and (b) GI MS processes.

Surface topography and roughness were assessed based on AFM measurements. The surface of TiO₂ thin film deposited in the MF MS process (Figure 5a) had densely packed grains of ca. 30–50 nm size whose maximum height was equal to 30.3 nm. The root mean square (R_q) surface roughness was calculated with the use of WSxM v.5.0 software and was determined to be equal to 5.0 nm. Furthermore, the height distribution of grains was symmetric and thus exhibited good homogeneity of the surface. On the other hand, TiO₂ coatings deposited with GI MS were not composed of such pronounced grains; in their case, rather larger islands of ca. 300–500 nm in size with a maximum height of 23.3 nm were observed. Nevertheless, the R_q value was still quite low and equal to 3.5 nm.

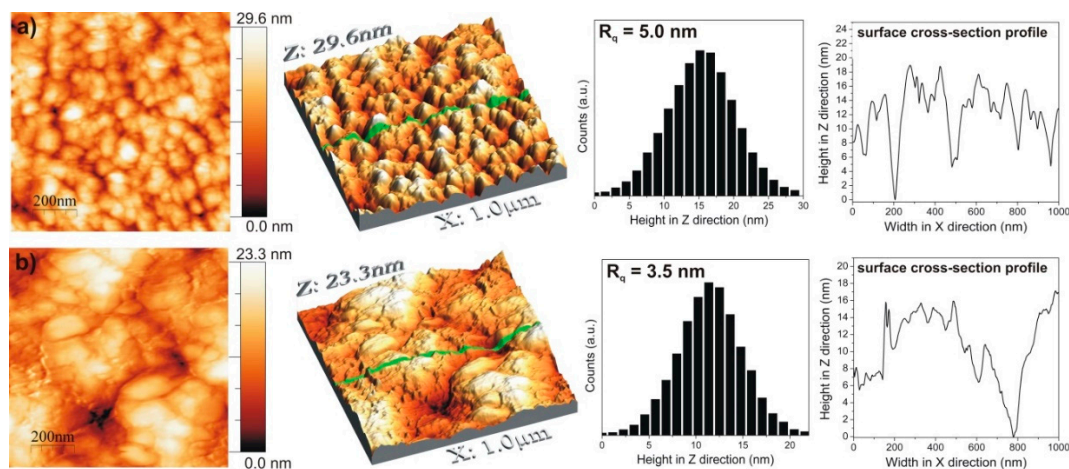


Figure 5. AFM images with high distribution of grain size in Z direction and cross-sectional topography of the as-prepared TiO₂ thin films from: (a) MF MS; (b) GI MS processes.

The XPS studies were performed in order to determine the oxidation states of titanium on the thin film surface and additionally to assess a possible change of the ability of coatings to adsorb hydroxyl groups and water molecules with the use of different sputtering techniques. The XPS spectra of Ti2p and O1s core levels are presented in Figure 6. The position of Ti2p doublet for thin films from MF MS and GI MS processes and the binding energy separation between the Ti2p_{3/2} and Ti2p_{1/2} peaks indicated that in both cases, the titanium was at the highest, +4 oxidation state. Moreover, the area ratio of the peaks related to Ti2p_{3/2} and Ti2p_{1/2} was equal to 2:1, thus confirming a good stoichiometry of the coatings. The results obtained for O1s state revealed that there was a difference in the amount of adsorbed water molecules (H₂O_{ads}) and hydroxyl radicals (OH⁻). The summarized level of adsorbed molecules, as compared to the whole signal obtained in the O1s region, was equal to 56.6% and 43.9% for TiO₂ deposited by MF MS and GI MS, respectively.

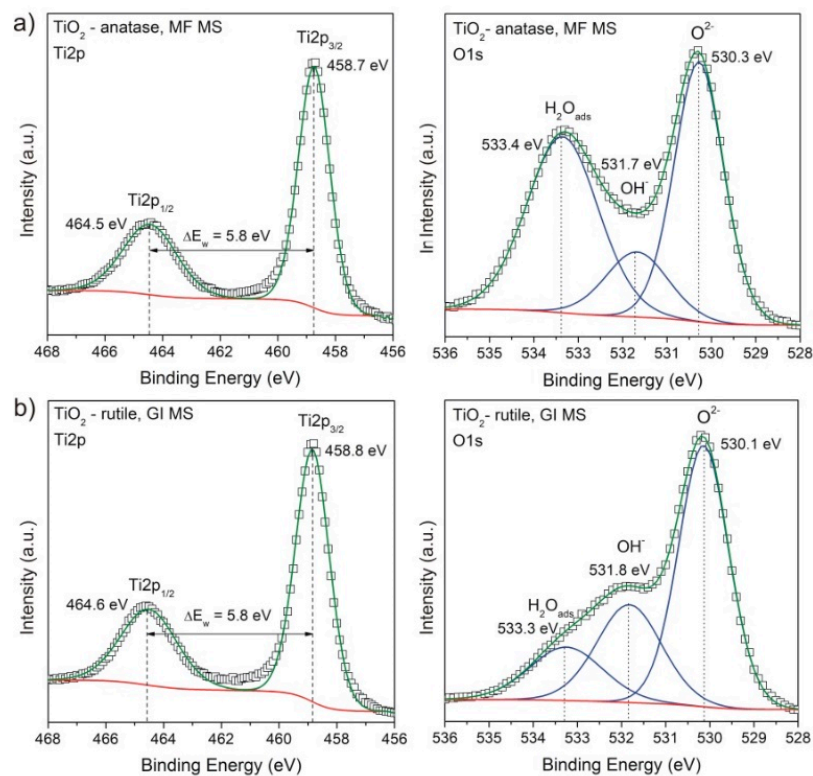


Figure 6. Ti2p and O1s core level XPS spectra of TiO₂ thin films obtained in: (a) MF MS; (b) GI MS processes.

Based on the water contact angle measurements, it was found that both TiO₂ thin films were hydrophilic, however, the wettability observed for the coating deposited by the MF MS process was significantly higher. The water contact angle was equal to 53.1° and 77.9° for TiO₂ prepared with the use of MF MS and GI MS processes, respectively (Figure 7). Similar results were obtained for ethylene glycol and ethanol; lower values were determined for films obtained by MF MS. Such contact angle values confirmed the analysis performed with the XPS method: with an increase of the adsorbed water molecules and hydroxyl radicals, the contact angle of each liquid decreased. The wettability analysis was completed with the use of the Zisman method [35,36] in which the application of a series of liquids with various surface tensions allows the plotting of the graph of cosθ vs. γ (Figure 7). Critical surface tension is often interpreted as the highest value of the surface tension of a liquid that will completely wet the thin film surface. In the case of as-deposited TiO₂ thin films, the lower value of the critical surface tension was determined for a coating obtained in the GI MS process, which finally confirmed that its surface was less wettable.

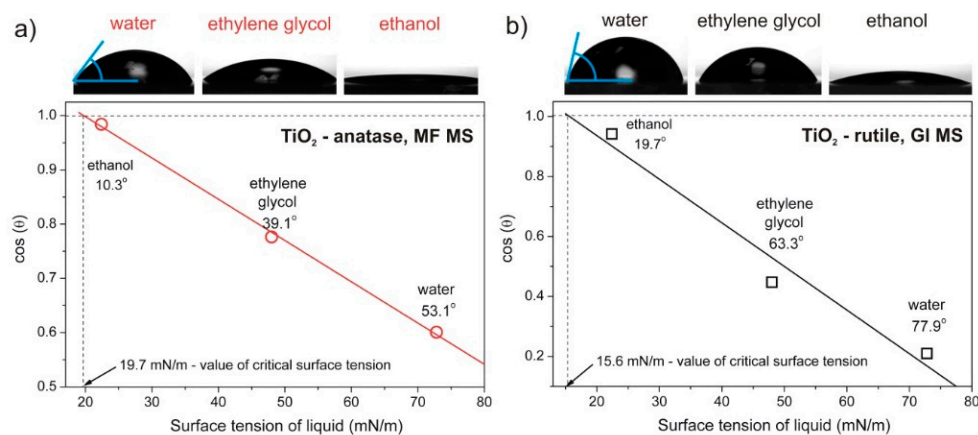


Figure 7. Results of wettability measurements with images of water, ethylene glycol, and ethanol droplets on the surface of TiO₂ thin films deposited by: (a) MF MS; (b) GI MS processes.

3.3. Optical Properties

The transmittance (T) and reflectance (R) measurements have shown that both thin films were transparent in the visible wavelength range with an average transmittance of ca. 80% (Figure 8a,b). Based on the obtained spectra, the characteristics of the refractive index (n) and extinction coefficient (k) were calculated with the use of FTG FilmStar software employing the extended Cauchy model for materials with $k > 0$. A higher value of the refractive index was determined for thin films with a rutile structure deposited by gas impulse magnetron sputtering and it was equal to 2.48 for a wavelength of 550 nm. In the case of TiO₂ thin films deposited by magnetron sputtering with a continuous gas flow, the n value was 2.20 at 550 nm (Figure 8c). With the use of optical modeling, it was also possible to estimate the extinction coefficient (Figure 8d). A lower value was obtained for the anatase sample, which might be related to the larger crystallites in its microstructure. Therefore, the light passing through the sample would encounter fewer light-scattering centers than in the case of the rutile film composed of very small crystallites in an amorphous shell. However, it is also worth emphasizing that the extinction coefficient in both cases was lower than 10^{-2} , which is quite a good value for high-quality optical coatings.

To assess the position of the fundamental absorption edge ($_{cut-off}$), optical band gap energy (E_g^{opt}), and Urbach energy (E_U), the transmission spectra were measured perpendicular to the samples. The results showed that in the case of the fundamental absorption edge, there was almost no shift in its position between the anatase and rutile thin films (Figure 9a) and it was in the range from 342 to 346 nm, respectively. The optical band gap energy was evaluated based on Tauc plots $(h\nu)^{1/2}$ as a function of photon energy (eV) for indirect transitions (Figure 9b). Analysis results revealed that the TiO₂-rutile coating had a lower optical band gap of 0.1 eV than the anatase one and it was equal to 3.08 eV. The Urbach energy was determined from the plot of $\ln(\alpha)$ as a function of photon energy (Figure 9c). It was found that the lower value of E_U was obtained for the anatase thin film, which was directly related to the significantly more ordered structure of this coating as stated during the microstructure analysis.

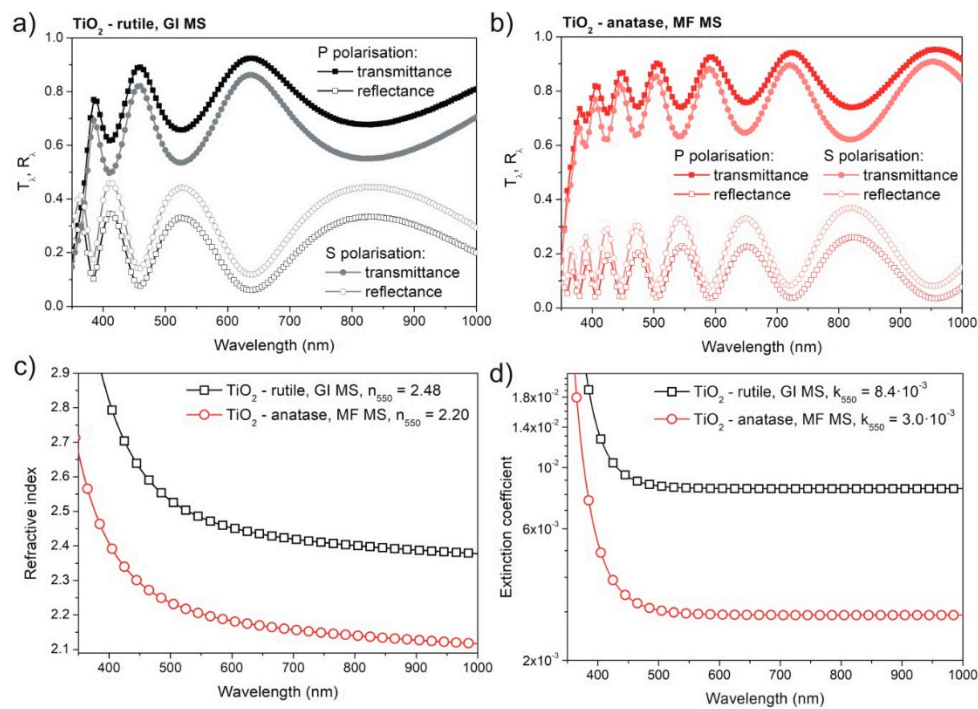


Figure 8. Transmittance and reflectance spectra taken for S and P polarization of 30° of light incidence for as-prepared TiO₂ thin films from: (a) MF MS; (b) GI MS processes; (c) comparison of refractive index; (d) comparison of extinction coefficient.

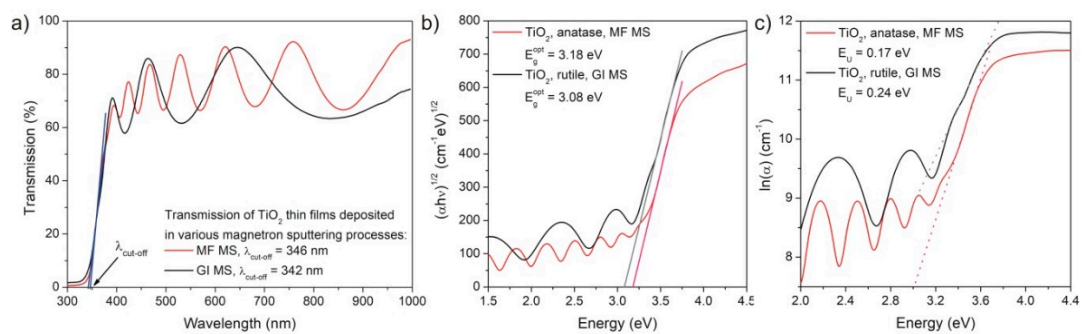


Figure 9. Comparison of: (a) transmittance spectra; (b) optical energy band gap; (c) Urbach energy of as-deposited TiO₂ thin films from MF MS and GI MS processes.

3.4. Mechanical Properties

The results of nanoindentation tests are shown in Figure 10. The x -axis is denoted as a relative indenter displacement with h/g ratio, where g is the thin film thickness and h is the displacement of the indenter into the thin film. The hardness of TiO₂ thin film deposited in the MF MS process was equal to 4.8 GPa, while for the coating obtained in the GI MS process, it was 16.1 GPa. Similarly, Young’s elastic modulus was lower for the thin film from the MF MS than for the GI MS process and equal to 114.4 and 139.3 GPa, respectively.

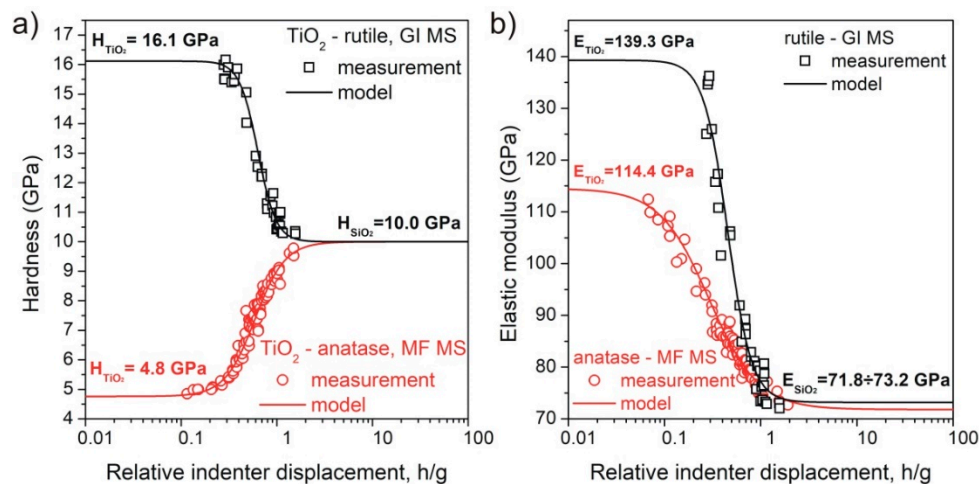


Figure 10. Results of hardness and elastic modulus investigations of as-prepared TiO₂ thin films from: (a) MF MS; (b) GI MS.

In the case of the tribological performance of the thin films, the resistance against elastic strain to failure can be evaluated based on nanoindentation results of hardness (H) and Young's elastic modulus (E), taking into consideration the H^3/E^2 ratio. The high value of such a plasticity index (i.e., high hardness and low elastic modulus) can indicate coatings with higher strength [37,38]. Due to the much higher hardness of the thin film deposited by the GI MS process, this coating also exhibited better mechanical performance. The H^3/E^2 ratio for thin films from the GI MS and MF MS processes were equal to 0.215 and 0.008, respectively.

In the case of protective transparent coatings which may be applied in the field of ophthalmics, optoelectronics, or windows, their tribological properties are also crucial. The results of the oscillating sand test is presented in Figure 11. In the case of both as-deposited TiO₂ thin films before performing the scratch test (Figure 11, left side), their surface was homogenous, smooth, and without visible scratches. The root mean square height (S_q) parameter was equal to 1.0 nm and 1.2 nm for TiO₂ deposited by the MF MS and GI MS processes, respectively. In the case of thin films prepared with the use of MF MS, their surface after performing the oscillating sand test changed significantly (Figure 11a, right side). Based on the images obtained with the use of an optical microscope and an optical profiler, it can be stated that this coating is not protective against scratches and exhibited rather poor scratch resistance. The S_q parameter increased significantly up to 45.1 nm due to a visible failure of the surface. Opposite results were obtained for the rutile thin film deposited by the gas impulse magnetron sputtering process. Its surface was unscratched and the S_q value increased negligibly to 1.4 nm, hence proving very good scratch resistance and protective properties of this thin film.

Figure 12 shows a comparison of surface cross-sectional profiles of the deposited thin films before and after abrasion tests. In the case of TiO₂ coating with anatase phase obtained in the MF MS process, it is clearly seen that after the oscillating sand test, the surface of the thin film was severely damaged with the maximum depth of scratches reaching even 300 nm. In the case of the rutile coating, its surface cross-sectional profile still looked almost the same as before the test and no scratches were visible. These studies confirmed that the mechanical performance obtained for TiO₂ thin films deposited with the gas impulse magnetron sputtering technique was significantly better.

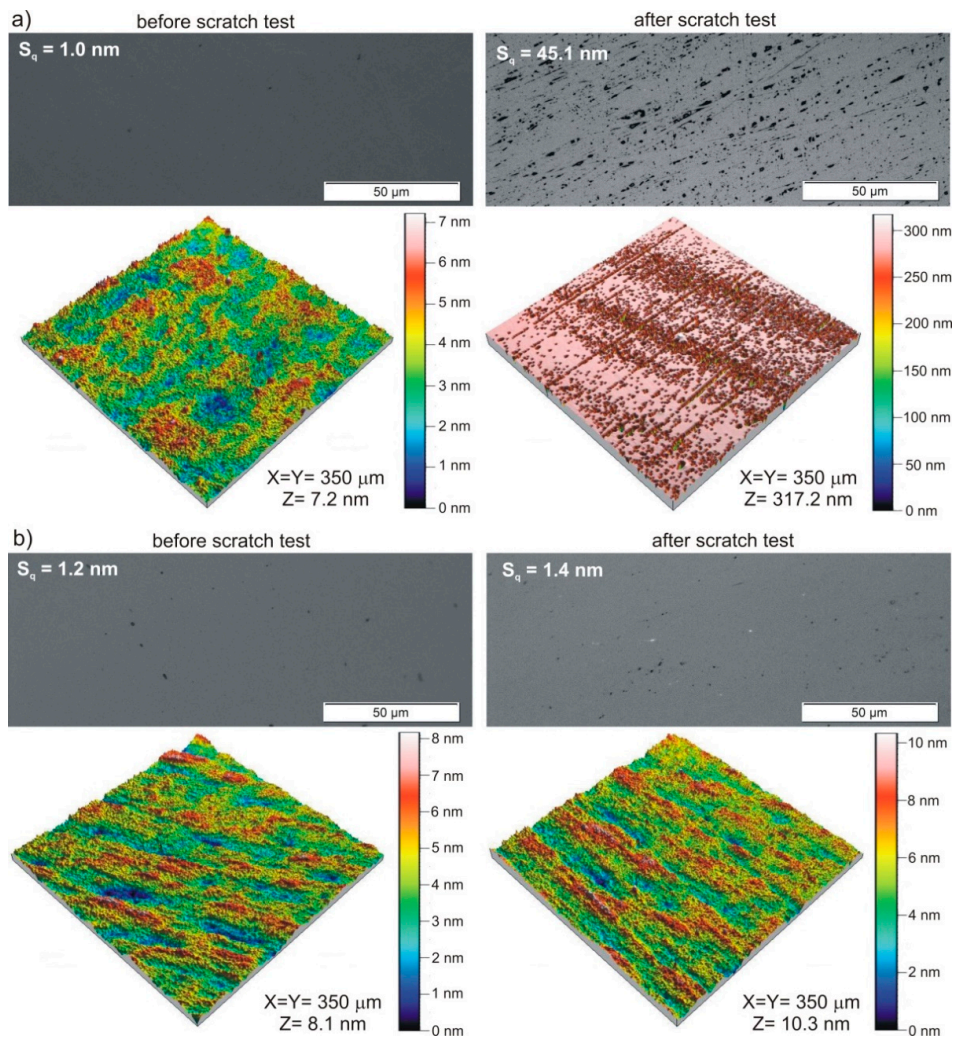


Figure 11. Optical microscope and profiler images of the surface of thin films before and after scratch test deposited by: (a) MF MS; (b) GI MS processes.

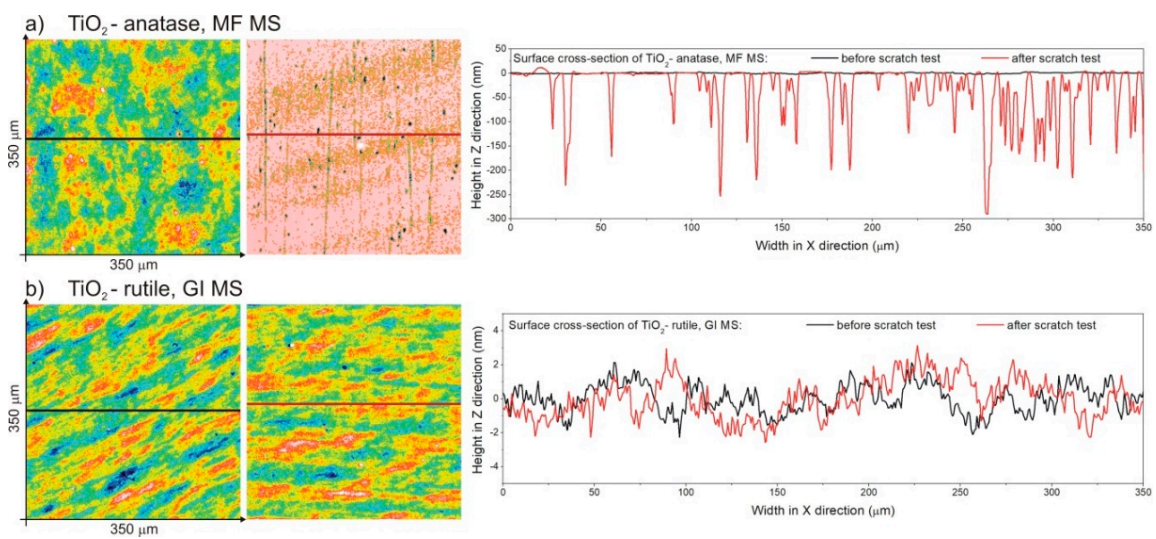


Figure 12. Surface cross-sectional profiles of thin films before and after scratch test deposited by: (a) MF MS; (b) GI MS.

4. Discussion

Two sets of titanium dioxide thin films were deposited using medium frequency and gas impulse magnetron sputtering techniques. In order to determine the differences of the sputtered coatings, suitable structural, surface, optical, and mechanical studies were performed. The change of the gas-supplying mode from continuous to pulsed strongly affected not only the thickness of the thin films, but also their microstructure and therefore the optical and mechanical properties. It was shown that the change of the gas-supplying mode was beneficial as much higher hardness and also significantly better scratch resistance were obtained as a result. It is worth emphasizing that such findings are unique, because they show the direct impact of the gas flow mode on the microstructure and relate it to the stoichiometry of thin films and their optical and mechanical properties.

The analysis of the microstructure investigations revealed that thin films deposited by MF MS and GI MS had an anatase and rutile phase, respectively. The former had a fibrous structure with an average crystallite size of 36 nm, while the latter had grainy structure with crystallites of 11 nm. It was found that nanocrystallites of the rutile thin film were much more defective as compared to the anatase coating. It was possible to obtain the TiO₂-rutile phase directly during the deposition process because of much lower pressure in the vacuum chamber, which resulted from the pulsed gas supply. Therefore, during the sputtering, Ti species reaching the substrates had a much higher kinetic energy due to the lower number of collisions with residual gas present in the chamber.

The investigation of surface properties showed that both thin films exhibited low roughness of a few nanometers, which is favorable in the case of optical coatings. In such a situation, the smooth surface of thin films does not provide additional light scattering centers which could increase the absorption or reflection of light incidenting at the coating. Additionally, the analysis of the chemical state of the surface revealed that the titanium was at +4 oxidation state in the case of both coatings. The ability to adsorb water molecules and hydroxyl radicals analyzed with the use of XPS was higher for the thin films deposited by MF MS, which had a direct impact on better wettability as compared to the one prepared by GI MS. Moreover, both coatings were hydrophilic.

Optical properties were analyzed with the use of transmittance and reflectance measurements. Both thin films were transparent in the visible wavelength range and had a relatively low extinction coefficient, while a much higher refractive index and thus also packing density were obtained for thin films deposited with the GI MS process. Based on the refractive index value, the packing density of thin films was determined [39,40] to directly compare coatings made of the same material but different crystal phases. This correlation can be expressed with the use of following Equation (1):

$$P = \frac{(n_f^2 - 1) \cdot (n_b^2 + 1)}{(n_f^2 + 2) \cdot (n_b^2 - 1)} \quad (1)$$

where: n_f —refractive index of thin films at 550 nm, n_b —refractive index of bulk TiO₂ (depending on the crystal phase) at 550 nm. Taking into consideration Equation (1), the calculated packing density of TiO₂ deposited by the GI MS and MF MS processes was equal to 0.95 and 0.86, respectively. These results are consistent with previous TEM studies which revealed a fibrous microstructure with voids in the case of the anatase thin film, while for the rutile one, the microstructure was denser and composed of small nanocrystallites. Moreover, the difference of the fundamental absorption edge between the anatase and rutile coatings was rather negligible, however, slightly lower optical band gap energy was observed for the rutile film.

In the case of mechanical performance, it was found that the thin films obtained in the GI MS process were significantly harder than the ones from MF MS process. This had also an impact on the H^3/E^2 ratio, which was considerably greater for the rutile coating. It is worth emphasizing that the hardness value should be well correlated with thin film density. Therefore, the coating with higher packing density, that is, TiO₂ deposited in the GI MS process, exhibited higher hardness. The performed

investigations of the microstructure revealed that in the case of TiO₂-rutile thin films deposited by gas impulse magnetron sputtering, the coating was in fact a nanocomposite where very small crystallites of nanometer size were surrounded by amorphous shells. Moreover, its microstructure was much more defective. Therefore, it can be assumed that the crystalline–amorphous nanocomposite system and the presence of the amorphous TiO₂ phase in the crystallite boundaries can have an advantageous impact on the hardness of thin films. It might be due to stress relaxation which is generated by dislocations on the surface of crystallites and thus the deformation during nanoindentation may not cause such severe deformation of the adjacent areas [41,42]. Therefore, the macroscopic plastic deformation of the rutile thin film may be much more difficult than in the case of the anatase coating, which leads to much higher hardness and significantly better scratch resistance. Similar results, as in the case of hardness, were obtained for scratch resistance investigations. In this case, the measurements of the surface of the anatase thin film showed that it was severely damaged, while the rutile one remained unscratched.

Based on the performed investigations, it can be stated that the thin films deposited with a gas impulse magnetron sputtering had a nanocrystalline, densely packed rutile structure with a smooth and hydrophilic surface. The GI MS deposition process used in this work allowed the obtaining of thin films with good optical properties, very high hardness, and excellent scratch resistance.

5. Conclusions

In this paper, a comparison of TiO₂ thin films prepared by magnetron sputtering with a continuous and pulsed gas flow was described. It was found that thin films deposited with a gas impulse had a nanocrystalline TiO₂-rutile structure instead of the fibrous-like TiO₂-anatase one obtained with the continuous distribution of gas. Films deposited with both techniques were transparent in the visible wavelength range, however, a significantly higher refractive index and packing density were observed for coatings deposited by the gas pulsed technique. The application of gas impulse increased the hardness of the TiO₂ coating more than three times and was also favorable in the case of scratch resistance.

Author Contributions: Conceptualization, A.W., M.M. and D.K.; Methodology, A.W., M.M. and D.W.; Formal Analysis, A.W., M.M., D.W., D.K., J.M. and D.G.; Investigation, A.W., M.M., A.O., D.W. and J.M.; Visualization, A.W., M.M., A.O. and D.W.; Original Draft Preparation, M.M.; Review & Editing, A.W. and M.M.; Supervision, D.K.; Funding Acquisition, M.M. and D.K.

Funding: This research was financed from the sources granted by the Polish National Science Centre NCN, research project number DEC-2013/09/B/ST8/00140. The authors would also like to acknowledge the financial support from Polish Ministry of Science and Higher Education within the “IUVENTUS Plus” program no. IP2014 029473 in the years 2015–2017.

Conflicts of Interest: The authors declare no conflict of interest.

References

1. Nezar, S.; Saoul, N.; Sali, S.; Faiz, M.; Mekki, M.; Laoufi, N.A.; Tabet, N. Properties of TiO₂ thin films deposited by rf reactive magnetron sputtering on biased substrates. *Appl. Surf. Sci.* **2017**, *395*, 172–179. [[CrossRef](#)]
2. Vyas, S.; Tiwary, R.; Shubham, K.; Chakrabarti, P. Study the target effect on the structural, surface and optical properties of TiO₂ thin film fabricated by RF sputtering method. *Superlattices Microstruct.* **2015**, *80*, 215–221. [[CrossRef](#)]
3. Miller, M.J.; Wang, J. Coupled effects of deposition and annealing temperatures on optical, electrical and mechanical properties of titanium oxide thin films. *Vacuum* **2015**, *120*, 155–161. [[CrossRef](#)]
4. Choi, K.H.; Duraisamy, N.; Muhammad, N.M.; Kim, I.; Choi, H.; Jo, J. Structural and optical properties of electrohydrodynamically atomized TiO₂ nanostructured thin films. *Appl. Phys. A* **2012**, *107*, 715–722. [[CrossRef](#)]
5. Wang, H.; Li, Y.; Ba, X.; Huang, L.; Yu, Y. TiO₂ thin films with rutile phase prepared by DC magnetron co-sputtering at room temperature: Effect of Cu incorporation. *Appl. Surf. Sci.* **2015**, *345*, 49–56. [[CrossRef](#)]

6. Lin, J.; Wang, B.; Sproul, W.D.; Ou, Y.; Dahan, I. Anatase and rutile TiO₂ films deposited by arc-free deep oscillation magnetron sputtering. *J. Phys. D Appl. Phys.* **2013**, *46*, 084008. [[CrossRef](#)]
7. Anders, A. Fundamentals of pulsed plasmas for materials processing. *Surf. Coat. Technol.* **2004**, *183*, 301–311. [[CrossRef](#)]
8. Wiatrowski, A.; Posadowski, W.M.; Jóźwiak, G.; Serafińczuk, J.; Szeloch, R.; Gotszalk, T. Standard and self-sustained magnetron sputtering deposited Cu films investigated by means of AFM and XRD. *Microelectron. Reliab.* **2011**, *51*, 1203–1206. [[CrossRef](#)]
9. Anders, A. Deposition rates of high power impulse magnetron sputtering: Physics and economics. *J. Vac. Sci. Technol. A* **2010**, *28*, 783–790. [[CrossRef](#)]
10. Anders, A. Discharge physics of high power impulse magnetron sputtering. *Surf. Coat. Technol.* **2011**, *205*, S1–S9. [[CrossRef](#)]
11. Wiatrowski, A.; Kijaszek, W.; Posadowski, W.M.; Oleszkiewicz, W.; Jadczak, J.; Kunicki, P. Deposition of diamond-like carbon films by the high power impulse magnetron sputtering method. *Diamond Relat. Mater.* **2017**, *72*, 71–76. [[CrossRef](#)]
12. Vlček, J.; Rezek, J.; Houška, J.; Kozák, T.; Kohout, J. Benefits of the controlled reactive high-power impulse magnetron sputtering of stoichiometric ZrO₂ films. *Vacuum* **2015**, *114*, 131–141. [[CrossRef](#)]
13. Vlček, J.; Belosludtsev, A.; Rezek, J.; Houška, J.; Čapek, J.; Čerstvý, R.; Haviar, S. High-rate reactive high-power impulse magnetron sputtering of hard and optically transparent HfO₂ films. *Surf. Coat. Technol.* **2016**, *290*, 58–64. [[CrossRef](#)]
14. Wiatrowski, A.; Patela, S.; Kunicki, P.; Posadowski, W. Effective pulsed magnetron sputtering of aluminium oxide—Properties of films deposited utilizing automated process stabilizer. *Vacuum* **2016**, *134*, 54–62. [[CrossRef](#)]
15. Posadowski, W.M.; Wiatrowski, A.; Dora, J.; Radzimski, Z.J. Magnetron sputtering process control by medium-frequency power supply parameter. *Thin Solid Films* **2008**, *516*, 4478–4482. [[CrossRef](#)]
16. Skowronski, L.; Zdunek, K.; Nowakowska-Langier, K.; Chodun, R.; Trzcinski, M.; Kobierski, M.; Kustra, M.K.; Wachowiak, A.A.; Wachowiak, W.; Hiller, T.; et al. Characterization of microstructural, mechanical and optical properties of TiO₂ layers deposited by GIMS and PMS methods. *Surf. Coat. Technol.* **2015**, *282*, 16–23. [[CrossRef](#)]
17. Zdunek, K.; Nowakowska-Langier, K.; Chodun, R.; Dora, J.; Okrasa, S.; Talik, E. Optimization of gas injection conditions during deposition of AlN layers by novel reactive GIMS method. *Mater. Sci.-Pol.* **2014**, *32*, 171–175. [[CrossRef](#)]
18. Zdunek, K.; Nowakowska-Langier, K.; Dora, J.; Chodun, R. Gas injection as a tool for plasma process control during coating deposition. *Surf. Coat. Technol.* **2013**, *228*, S367–S373. [[CrossRef](#)]
19. Zdunek, K.; Skowronski, L.; Chodun, R.; Nowakowska-Langier, K.; Grabowski, A.; Wachowiak, W.; Okrasa, S.; Wachowiak, A.; Strauss, O.; Wronkowski, A.; et al. Novel GIMS technique for deposition of colored Ti/TiO₂ coatings on industrial scale. *Mater. Sci.-Pol.* **2016**, *34*, 137–141. [[CrossRef](#)]
20. Bukauskas, V.; Kaciulis, S.; Mezzi, A.; Mironas, A.; Niaura, G.; Rudzikas, M.; Šimkienė, I.; Šetkus, A. Effect of substrate temperature on the arrangement of ultra-thin TiO₂ films grown by a dc-magnetron sputtering deposition. *Thin Solid Films* **2015**, *585*, 5–12. [[CrossRef](#)]
21. Roy, S.S.; Bhuiyan, A.H. Surface morphology, compositional, optical and electrical properties of TiO₂ thin films. *Sens. Transducers J.* **2015**, *192*, 66–73.
22. Jiang, S.S.; Hea, G.; Gao, J.; Xiao, D.Q.; Jin, P.; Li, W.D.; Lv, J.G.; Liu, M.; Liu, Y.M.; Sun, Z.Q. Microstructure, optical and electrical properties of sputtered HfTiO high-k gate dielectric thin films. *Ceram. Int.* **2016**, *42*, 11640–11649. [[CrossRef](#)]
23. Jin, P.; He, G.; Liu, M.; Xiao, D.Q.; Gao, J.; Chen, X.F.; Ma, R.; Zhang, J.W.; Zhang, M.; Sun, Z.Q.; et al. Deposition-power-modulated optical and electrical properties of sputtering-derived HfTiO_x gate dielectrics. *J. Alloy. Compd.* **2015**, *649*, 128–134. [[CrossRef](#)]
24. Oliver, W.C.; Pharr, G.M. An improved technique for determining hardness and elastic modulus using load and displacement sensing indentation experiments. *J. Mater. Res.* **1992**, *7*, 1564–1583. [[CrossRef](#)]
25. ASTM F735-17 Standard Test Method for Abrasion Resistance of Transparent Plastics and Coatings Using the Oscillating Sand Method; ASTM International: West Conshohocken, PA, USA, 2017.
26. JCPDS Card 21-1276 Powder Diffraction File; Joint Committee on Powder Diffraction Standards: Swarthmore, PA, USA, 1967.

27. JCPDS Card 21-1272 Powder Diffraction File; Joint Committee on Powder Diffraction Standards: Swarthmore, PA, USA, 1967.
28. Domaradzki, J.; Kaczmarek, D.; Prociow, E.L.; Wojcieszak, D.; Sieradzka, K.; Mazur, M.; Lapinski, M. Study of structural and optical properties of TiO₂:Tb thin films prepared by high energy reactive magnetron sputtering method. *Optica Applicata* **2009**, *39*, 815–823.
29. Wojcieszak, D.; Mazur, M.; Kaczmarek, D.; Morgiel, J.; Zatoryb, G.; Domaradzki, J.; Misiewicz, J. Influence of Nd dopant amount on microstructure and photoluminescence of TiO₂:Nd thin films. *Opt. Mater.* **2015**, *48*, 172–178. [[CrossRef](#)]
30. Mazur, M.; Wojcieszak, D.; Domaradzki, J.; Kaczmarek, D.; Poniedzialek, A.; Domanowski, P. Investigation of microstructure, micro-mechanical and optical properties of HfTiO₄ thin films prepared by magnetron co-sputtering. *Mater. Res. Bull.* **2015**, *72*, 116–122. [[CrossRef](#)]
31. Danish, R.; Ahmed, F.; Arshi, N.; Anwar, M.S.; Koo, B.H. Facile synthesis of single crystalline rutile TiO₂ nano-rods by solution method. *Trans. Nonferrous Met. Soc. China* **2014**, *24*, s152–s156. [[CrossRef](#)]
32. Alhomoudi, I.A.; Newaz, G. Residual stresses and Raman shift relation in anatase TiO₂ thin film. *Thin Solid Films* **2009**, *517*, 4372–4378. [[CrossRef](#)]
33. Gupta, S.K.; Singh, J.; Anbalagan, K.; Kothari, P.; Bhatia, R.R.; Mishra, P.K.; Manjuladevi, V.; Gupta, R.K.; Akhtar, J. Synthesis, phase to phase deposition and characterization of rutile nanocrystalline titanium dioxide (TiO₂) thin films. *Appl. Surf. Sci.* **2013**, *264*, 737–742. [[CrossRef](#)]
34. Kadam, R.M.; Rajeswari, B.; Sengupta, A.; Achary, S.N.; Kshirsagar, R.J.; Natarajan, V. Structural characterization of titania by X-ray diffraction, photoacoustic, Raman spectroscopy and electron paramagnetic resonance spectroscopy. *Spectrochim. Acta Part A* **2015**, *137*, 363–370. [[CrossRef](#)] [[PubMed](#)]
35. Kwok, D.Y.; Neumann, A.W. Contact angle measurement and contact angle interpretation. *Adv. Colloid Interface Sci.* **1999**, *81*, 167–249. [[CrossRef](#)]
36. Sharfrin, E.; Zisman, W.A. Constitutive relations in the wetting of low energy surfaces and the theory of the retraction method of preparing monolayer. *J. Phys. Chem.* **1960**, *64*, 519–524. [[CrossRef](#)]
37. Leyland, A.; Matthews, A. On the significance of the H/E ratio in wear control: a nanocomposite coating approach to optimized tribological behaviour. *Wear* **2000**, *246*, 1–11. [[CrossRef](#)]
38. Chang, L.C.; Chang, C.Y.; Chen, Y.I. Mechanical properties and oxidation resistance of reactively sputtered Ta_{1-x}Zr_xN_y thin films. *Surf. Coat. Technol.* **2015**, *280*, 27–36. [[CrossRef](#)]
39. Dave, V.; Dubey, P.; Gupta, H.O.; Chandra, R. Influence of sputtering pressure on the structural, optical and hydrophobic properties of sputtered deposited HfO₂ coatings. *Thin Solid Films* **2013**, *549*, 2–7. [[CrossRef](#)]
40. Bauer, G. Absolutwerte der optischen Absorptionskonstanten von Alkalihalogenidkristallen im Gebiet ihrer ultravioletten Eigenfrequenzen. *Ann. Phys.* **1934**, *411*, 434–464. [[CrossRef](#)]
41. Patschaider, J. Nano-composite hard coatings for wear protection. *MRS Bull.* **2003**, *28*, 180–183. [[CrossRef](#)]
42. Vepřek, S.; Reiprich, S. A concept for the design of novel superhard coatings. *Thin Solid Films* **1995**, *268*, 64–71. [[CrossRef](#)]

